Hydrology and
Earth System
Sciences

An improved SWAT vegetation growth module and its evaluation for four tropical ecosystems

Tadesse Alemayehu[1,2], Ann van Griensven[1,2], Befekadu Taddesse Woldegiorgis[1], and Willy Bauwens[1]

[1]Vrije Universiteit Brussel (VUB), Department of Hydrology and Hydraulic Engineering, Brussels, Belgium
[2]IHE Delft Institute for Water Education, Department of Water Science and Engineering, Delft, the Netherlands

Correspondence to: Tadesse Alemayehu (t.abitew@un-ihe.org)

Abstract. The Soil and Water Assessment Tool (SWAT) is a globally applied river basin ecohydrological model used in a wide spectrum of studies, ranging from land use change and climate change impacts studies to research for the development of the best water management practices. However, SWAT has limitations in simulating the seasonal growth cycles for trees and perennial vegetation in the tropics, where rainfall rather than temperature is the dominant plant growth controlling factor. Our goal is to improve the vegetation growth module of SWAT for simulating the vegetation variables – such as the leaf area index (LAI) – for tropical ecosystems. Therefore, we present a modified SWAT version for the tropics (SWAT-T) that uses a straightforward but robust soil moisture index (SMI) – a quotient of rainfall (P) and reference evapotranspiration (ET_r) – to dynamically initiate a new growth cycle within a predefined period. Our results for the Mara Basin (Kenya/Tanzania) show that the SWAT-T-simulated LAI corresponds well with the Moderate Resolution Imaging Spectroradiometer (MODIS) LAI for evergreen forest, savanna grassland and shrubland. This indicates that the SMI is reliable for triggering a new annual growth cycle. The water balance components (evapotranspiration and streamflow) simulated by the SWAT-T exhibit a good agreement with remote-sensing-based evapotranspiration (ET-RS) and observed streamflow. The SWAT-T model, with the proposed vegetation growth module for tropical ecosystems, can be a robust tool for simulating the vegetation growth dynamics in hydrologic models in tropical regions.

1 Introduction

The Soil and Water Assessment Tool (SWAT; Arnold et al., 1998) is a process-oriented, spatially semi-distributed and time-continuous river basin model. SWAT is one of the most widely applied ecohydrological models for the modelling of hydrological and biophysical processes under a range of climate and management conditions (Arnold et al., 2012; Bressiani et al., 2015; Gassman et al., 2014; van Griensven et al., 2012; Krysanova and White, 2015). SWAT has been used in many studies in tropical Africa to investigate the basin hydrology (e.g. Dessu and Melesse, 2012; Easton et al., 2010; Mwangi et al., 2016; Setegn et al., 2009) as well as to study the hydrological impacts of land use change (e.g. Gebremicael et al., 2013; Githui et al., 2009; Mango et al., 2011) and climate change (Mango et al., 2011; Mengistu and Sorteberg, 2012; Setegn et al., 2011; Teklesadik et al., 2017). Notwithstanding the high number of SWAT model applications in tropical catchments, only a few studies discussed the limitation of its plant growth module for simulating the growth cycles of trees and of perennial and annual vegetation in this region of the world (Mwangi et al., 2016; Strauch and Volk, 2013; Wagner et al., 2011).

It is worthwhile to note that phenological changes in vegetation affect the biophysical and hydrological processes in the basin and thus play a key role in integrated hydrologic and ecosystem modelling (Jolly and Running, 2004; Kiniry and MacDonald, 2008; Shen et al., 2013; Strauch and Volk, 2013; Yang and Zhang, 2016; Yu et al., 2016). The leaf area index (LAI) – the area of green leaves per unit area of land – is a vegetation attribute commonly used in ecohydrological modelling, as it strongly correlates with the vegetation phe-

nological development. Thus, an enhanced representation of the LAI dynamics can improve the predictive capability of hydrologic models, as already noted in several studies (Andersen et al., 2002; Yu et al., 2016; Zhang et al., 2009). Arnold et al. (2012) underscored the need for a realistic representation of the local and regional plant growth processes to reliably simulate the water balance, the erosion and the nutrient yields using SWAT. For instance, the LAI and canopy height are needed to determine the canopy resistance and the aerodynamic resistance to subsequently compute the potential plant transpiration in SWAT. Therefore, inconsistencies in the vegetation growth simulations could result in uncertain estimates of the actual evapotranspiration (ET), as noted in Alemayehu et al. (2015).

SWAT utilizes a simplified version of the Environmental Policy Impact Climate (EPIC) crop growth module to simulate the phenological development of plants, based on accumulated heat units (Arnold et al., 1998; Neitsch et al., 2011). It uses dormancy, which is a function of day length and latitude, to repeat the annual growth cycle for trees and perennials. Admittedly, this approach is suitable for temperate regions. However, Strauch and Volk (2013) showed that the temporal dynamics of the LAI are not well represented for perennial vegetation (savanna and shrubs) and evergreen forest in Brazil. Likewise, Wagner et al. (2011) reported a mismatch between the growth cycle of deciduous forest and the SWAT dormancy period in the Western Ghats (India), and they subsequently shifted the dormancy period to the dry season.

Unlike temperate regions where the vegetation growth dynamics are mainly controlled by the temperature, the primary controlling factor in tropical regions is the rainfall (i.e. the water availability) (Jolly and Running, 2004; Lotsch, 2003; Pfeifer et al., 2012, 2014; Zhang, 2005). A study of Zhang et al. (2005) explored the relationship between the rainfall seasonality and the vegetation phenology across Africa. They showed that the onset of the vegetation green-up can be predicted using the cumulative rainfall as a criterion for the season change. Jolly and Running (2004) determined the timing of leaf flush in an ecosystem process simulator (BIOME-BGC) after a defined dry season in the Kalahari, using events where the daily rainfall (P) exceeded the reference evapotranspiration (ET_r). They showed that the modelled leaf flush dates compared well with the leaf flush dates estimated from the normalized difference vegetation index (NDVI). This points to the feasibility of using a proxy derived from P and ET_r to pinpoint a season change in the tropics. Sacks et al. (2010) made a global study of the relations between crop planting dates and temperature, P and ET_r, using 30-year climatological values. They noted that in rainfall-limited regions the ratio of P to ET_r is a better proxy for the soil moisture status than P alone. Using a soil moisture index (SMI) derived from the ratio of P to ET_r to trigger a new growth cycle in hydrological modelling is appealing because the SMI can be determined a priori. On the other hand, Strauch and

Volk (2013) used the SWAT-simulated soil moisture in the top soil layers to indicate the start of a wet season (SOS) and thus of a new vegetation growth cycle. Their results showed an improved simulation of the seasonal dynamics of the LAI and a good match with the Moderate Resolution Imaging Spectroradiometer (MODIS) 8-day LAI. However, such an approach requires a calibration of the SWAT parameters that govern the soil water balance dynamics. The latter is not obvious when only observed streamflow data are used for the calibration (Yu et al., 2016).

The main objective of this study is to improve the vegetation growth module of SWAT for trees and perennials in the tropics. Towards this, the use of the SMI as a dynamic trigger for a new vegetation growth cycle within a predefined period will be explored. The modified SWAT (SWAT-T) model will be evaluated for the Mara River basin using 8-day MODIS LAI and remote-sensing-based ET (Alemayehu et al., 2017). Additionally, the model will be evaluated using observed daily streamflow data.

2 Materials and methods

2.1 The study area

The Mara River, a transboundary river shared by Kenya and Tanzania, drains an area of 13 750 km^2 (Fig. 1a). This river originates from the forested Mau Escarpment (about 3000 m a.s.l.). It meanders through diverse agroecosystems, subsequently crosses the Maasai Mara game reserve in Kenya and the Serengeti National Park in Tanzania and finally feeds Lake Victoria. The Amala River and the Nyangores River are its only perennial tributaries. The Talek River and the Sand River are the two most notable seasonal rivers stemming from Loita Hills.

Rainfall varies spatially mainly due to its equatorial location and the topography. The rainfall pattern in most part of the basin is bimodal, with a short rainy season (October–December) driven by convergence and southward migration of the Intertropical Convergence Zone (ITCZ) and a long rainy season (March–May) driven by south-easterly trades. In general, rainfall decreases from west to east across the basin, while temperature increases southwards. The Mara Basin is endowed with significant biodiversity features, including moist montane forest on the escarpment, dry upland forest, scattered woodland and extensive savanna grasslands (Fig. 1b). The upper forested basin is dominated by well-drained volcanic origin soils, while the middle and lower parts of the basin are dominated by poorly drained soil types with high clay content.

2.2 The SWAT model description

SWAT (Arnold et al., 1998, 2012; Neitsch et al., 2011) is a comprehensive, process-oriented and physically based eco-hydrological model for river basins. It requires specific in-
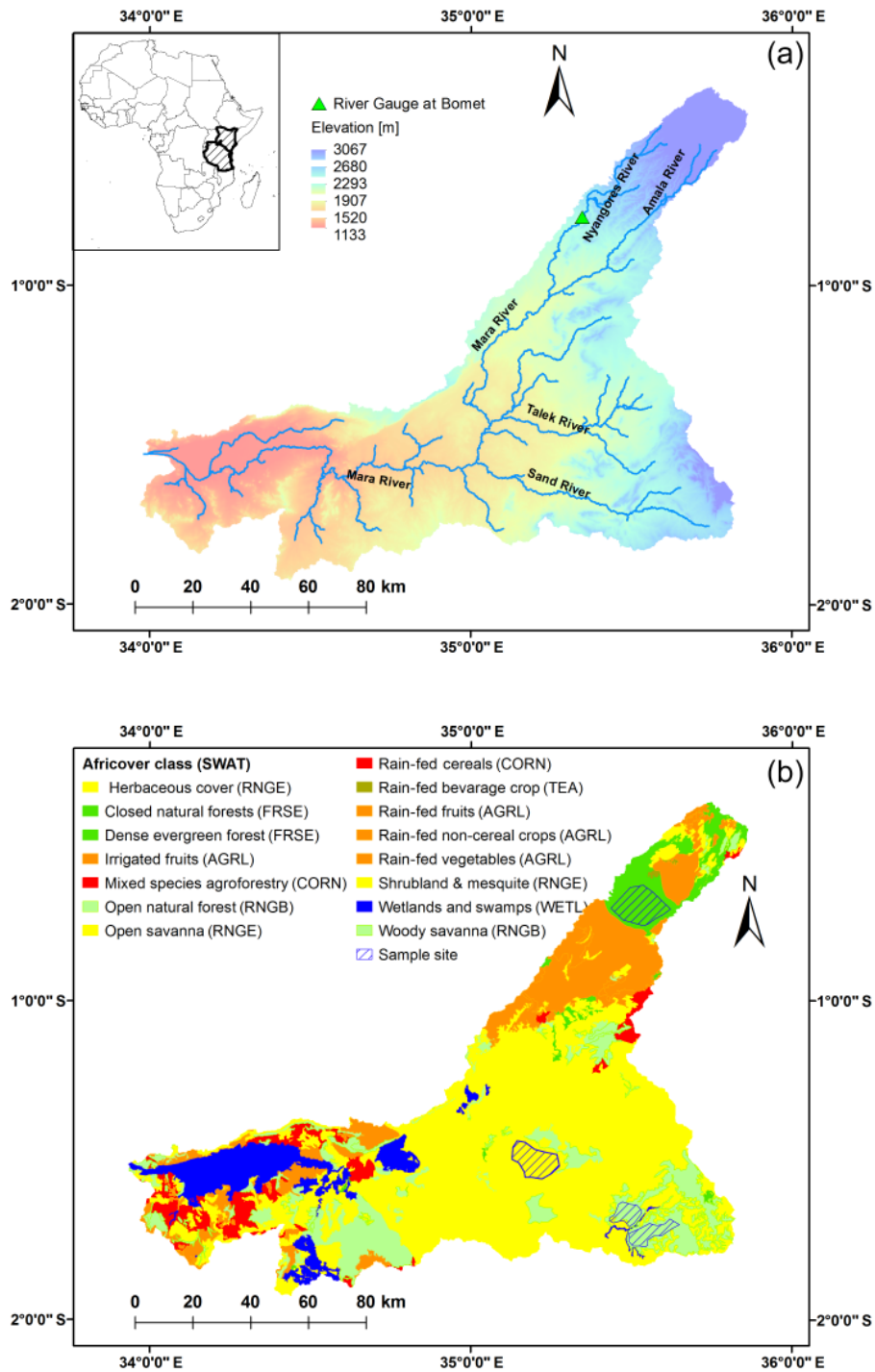
Figure 1. The Mara Basin **(a)** and its land cover classes **(b)**. Note the sample site locations (dashed areas) for the major natural vegetation classes that are used to mask the Moderate Resolution Imaging Spectroradiometer (MODIS) leaf area index (LAI).

formation about weather, soil properties, topography, vegetation and land management practices in the watershed to directly simulate physical processes associated with water movement, sediment movement, crop growth, nutrient cycling, etc. In SWAT, a basin is partitioned into sub-basins using topographic information. The sub-basins, in turn, are subdivided into hydrological response units (HRUs) that represent a unique combination of land use, soil type and slope class. All the hydrologic processes are simulated at HRU level on a daily or sub-daily time step. The flows are then

aggregated to sub-basin level for routing into a river network (Neitsch et al., 2011). SWAT considers five storages to calculate the water balance: snow, the canopy storage, the soil profile (with up to 10 layers), a shallow aquifer and a deep aquifer. The global water balance is expressed as

$$\Delta S = \sum_{i=1}^{N} (P - Q_{\text{total}} - \text{ET} - \text{losses}), \qquad (1)$$

where ΔS is the change in water storage (mm) and N is the time in days. P, Q_{total}, ET and losses are the amounts of precipitation (mm), the total water yield (mm), the evapotranspiration (mm) and the groundwater losses (mm), respectively. The total water yield represents an aggregated sum of the surface runoff, the lateral flow and the return flow. In this study, the surface runoff is computed using the Soil Conservation Service (SCS) curve number (CN) method (USDA SCS, 1972).

SWAT provides three options for estimating ET_r: the Hargreaves (Hargreaves and Samani, 1985), Priestley–Taylor (Priestley and Taylor, 1972) and Penman–Monteith (Monteith, 1965; Neitsch et al., 2011) methods. The model simulates evaporation from soil and plants separately, as described in Ritchie (1972). The potential soil evaporation is simulated as a function of ET_r and the LAI. The actual soil water evaporation is estimated by using exponential functions of soil depth and water content (Neitsch et al., 2011). The simulated LAI is also required to calculate the potential plant transpiration, with a formulation that varies depending on the selected ET_r method (Alemayehu et al., 2015; Neitsch et al., 2011). The actual plant transpiration (i.e. the plant water uptake) is reduced exponentially for soil water contents below field capacity. Therefore, the ET refers to the sum of the evaporation from the canopy and from the soil as well as plant transpiration.

In this study, we use the Penman–Monteith method (Monteith, 1965) to compute the ET_r for alfalfa reference crop as (Neitsch et al., 2011)

$$\text{ET}_r = \frac{\Delta \cdot (H_{\text{net}} - G) + \rho_{\text{air}} \cdot c_p \cdot \left[e_z^o - e_z\right]/r_a}{\Delta + \gamma \cdot (1 + r_c/r_a)}, \qquad (2)$$

where ET_r is the maximum transpiration rate (mm d^{-1}), Δ is the slope of the saturation vapour pressure–temperature curve (kPa °C^{-1}), H_{net} is the net radiation (MJ m^{-2} d^{-1}), G is the heat flux density to the ground (MJ m^{-2} d^{-1}), ρ_{air} is the air density (kg m^{-3}), C_p is the specific heat at constant pressure (MJ kg^{-1} °C^{-1}), e_z^0 is the saturation vapour pressure of air at height z (kPa), e_z is the water vapour pressure of air at height z (kPa), γ is the psychrometric constant (kPa °C^{-1}), r_c is the plant canopy resistance (s m^{-1}) and r_a is the diffusion resistance of the air layer (aerodynamic resistance) (s m^{-1}). The plant growth module in SWAT simulates the LAI and the canopy height, which are required to calculate the canopy and the aerodynamic resistance.

2.3 The vegetation growth and leaf area index modelling in SWAT

SWAT simulates the annual vegetation growth based on the simplified version of the EPIC plant growth model (Neitsch et al., 2011). The potential plant phenological development is hereby simulated on the basis of accumulated heat units under optimal conditions; however, the actual growth is constrained by temperature, water, nitrogen or phosphorous stress (Arnold et al., 2012; Neitsch et al., 2011).

Plant growth is primarily based on temperature, and hence each plant has its own temperature requirements (i.e. minimum, maximum and optimum). The fundamental assumption of the heat unit theory is that plants have a heat unit requirement that can be quantified and linked to the time of planting and maturity (Kiniry and MacDonald, 2008; Neitsch et al., 2011). The total number of heat units required for a plant to reach maturity must be provided by the user. The plant growth modelling includes the simulation of the leaf area development, the light interception and the conversion of intercepted light into biomass, assuming a plant species-specific radiation-use efficiency (Neitsch et al., 2011). The plant growth model assumes a uniform, single plant species community; thereby, plant mixtures such as trees and grass cannot be simulated in SWAT (Kiniry and MacDonald, 2008).

During the initial period of the growth, the optimal leaf area development is modelled (Neitsch et al., 2011) as

$$\text{fr}_{\text{LAI}_{\text{mx}}} = \frac{\text{fr}_{\text{PHU}}}{\text{fr}_{\text{PHU}} + \exp(l_1 - l_2 \cdot \text{fr}_{\text{PHU}})}, \qquad (3)$$

where $\text{fr}_{\text{LAI}_{\text{mx}}}$ is the fraction of the plant's maximum leaf area index corresponding to a given fraction of the potential heat units for the plant, fr_{PHU} is the fraction of potential heat units accumulated for the plant on a given day during the growing season, and l_1 and l_2 are shape coefficients. Once the maximum leaf area index is reached, the LAI will remain constant until the leaf senescence begins to exceed the leaf growth.

Afterwards, the leaf senescence becomes the dominant growth process, and hence the LAI follows a linear decline (Neitsch et al., 2011). However, Strauch and Volk (2013) suggested a logistic decline curve instead, in order to avoid the LAI dropping to zero before entering the dormancy stage. We adopted this change in SWAT2012, whereby the LAI during leaf senescence for trees and perennials is calculated as (Strauch and Volk, 2013)

$$\text{LAI} = \frac{\text{LAI}_{\text{mx}} - \text{LAI}_{\text{min}}}{1 + \exp(-t)} \qquad (4)$$

with $t = 12(r - 0.5)$

and $r = \dfrac{1 - \text{fr}_{\text{PHU}}}{1 - \text{fr}_{\text{PHU,sen}}}$, $\quad \text{fr}_{\text{PHU}} \geq \text{fr}_{\text{PHU,sen}}$,

where the term used as exponent is a function of time (t), and LAI_{mx} and LAI_{min} are the maximum and minimum (i.e.

during dormancy) leaf area index, respectively. $\mathrm{fr_{PHU,sen}}$ is the fraction of the potential heat units for the plant at which senescence becomes the dominant growth process and $\mathrm{fr_{PHU}}$ is the fraction of potential heat units accumulated for the plant on a given day during the growing season.

As detailed in Neitsch et al. (2011), the daily LAI calculations for perennials and trees are slightly different, as for the latter the years of development are considered.

For perennials, the LAI for a day i is calculated as

$$\mathrm{LAI}_i = \mathrm{LAI}_{i-1} + \Delta\mathrm{LAI}_i, \tag{5}$$

and the change of LAI on day i is calculated as

$$\Delta\mathrm{LAI}_i = \left(\mathrm{fr_{LAI_{mx}},_i} - \mathrm{fr_{LAI_{mx}},_{i-1}}\right) \cdot \mathrm{LAI_{mx}} \tag{6}$$
$$\cdot \left(1 - \exp(5 \cdot (\mathrm{LAI}_{i-1} - \mathrm{LAI_{mx}}))\right).$$

2.4 The limitation of the annual vegetation growth cycle simulation in SWAT for the tropics

Dormancy is the period during which trees and perennials do not grow. It is commonly considered to be a function of latitude and day length. It is assumed that dormancy starts as the day length nears the minimum day length of the year. At the beginning of the dormancy period, a fraction of the biomass is converted to residue and the leaf area index is set to the minimum value (Neitsch et al., 2011) and thereby resets the annual growth cycle. Also, SWAT offers two management settings options for the start and the end of the growing season, either based on a calendar date scheduling or based on heat units (the default).

In the tropics, however, dormancy is primarily controlled by precipitation (Bobée et al., 2012; Jolly and Running, 2004; Lotsch, 2003; Zhang et al., 2010; Zhang, 2005). Hence, the default growth module of SWAT cannot realistically represent the seasonal growth dynamics for trees and perennials in the tropics.

2.5 A soil moisture index-based vegetation growth cycle for the tropics

As several studies demonstrated (Jolly and Running, 2004; Zhang, 2005; Zhang et al., 2006), the water availability in the soil profile is one of the primary governing factors of the vegetation growth in the tropics. Thus, we propose to implement a soil moisture index (SMI) to trigger a new growth cycle for tropical ecosystems in SWAT within a predefined period. The SMI is computed as

$$\mathrm{SMI} = \frac{P}{\mathrm{ET_r}}, \tag{7}$$

where P and $\mathrm{ET_r}$ denote daily or aggregated rainfall and reference evapotranspiration ($\mathrm{mm\,d^{-1}}$), respectively. In this study, we used 5-day (i.e. pentad) aggregated P and $\mathrm{ET_r}$ to determine the SMI, in order to assure sufficient soil moisture availability to initiate a new growth cycle. The SMI is

somewhat similar to the water requirement satisfaction index (WRSI) (McNally et al., 2015; Verdin and Klaver, 2002), which is a ratio of ET to $\mathrm{ET_r}$.

Figure 2 presents the seasonal pattern of SMI, based on long-term precipitation for several gauge stations in the Mara Basin and $\mathrm{ET_r}$ data from Trabucco and Zomer (2009). It is apparent from Fig. 2 that the dry season (mostly from June to September) shows low SMI values (less than 0.5). Additionally, these patterns resemble well the long-term monthly average LAI for the savanna ecosystem (the dominant cover in the midsection of the Mara Basin). In areas with a humid climate (i.e. the headwater regions of the basin), the SMI values are high and the rainfall regime is different, yet in the relatively drier months (January and February) the SMI is low. As shown in Fig. 2, the LAI and the SMI seasonal dynamics match well, when a lag time of approximately 1 month is considered. From this, we conclude that the SMI can be used as a proxy for the start of the wet season (SOS) and hence to trigger the vegetation growth cycle. This approach enables a dynamic simulation of the growth cycle by SWAT, without the need to define the exact dates of the beginning and the end of the growing season (the "plant" and "kill" dates).

To avoid false starts of the new growing cycle during the dry season due to short-spell rainfall, the end of the dry season and the beginning of the rainy season ($\mathrm{SOS_1}$ and $\mathrm{SOS_2}$, respectively) should be provided by the user. These months are determined using a long-term monthly climatological P to $\mathrm{ET_r}$ ratio (Fig. 2). For a river basin with a single rainfall regime, a single set of SOS months are required. However, in a basin with multiple rainfall regimes (i.e. mostly large basins), different sets of SOS months should be provided at sub-basin level. In our study area, two distinct rainfall regimes are observed, and therefore two different SOS months were needed. For most sub-basins, October ($\mathrm{SOS_1}$) and November ($\mathrm{SOS_2}$) were used as transitions (Fig. 2).

2.6 The adaptation of the SWAT plant growth module in SWAT-T

Based on the rationale elaborated in the preceding sections, we modified the standard SWAT2012 (revision 627) plant growth subroutine for basins located between 20° N and 20° S:

i. If the simulation day is within $\mathrm{SOS_1}$ and $\mathrm{SOS_2}$ for a given HRU and a new growing cycle is not initiated yet, the SMI is calculated as the ratio of P to $\mathrm{ET_r}$.

ii. If the SMI exceeds or equals a user-defined threshold, a new growing cycle for trees and perennials is initiated. Subsequently, $\mathrm{fr_{PHU}}$ is set to 0 and the LAI is set to the minimum value. Plant residue decomposition and nutrient release is calculated as if dormancy would occur.

iii. In the case where the SMI is still below a user-defined threshold at the end of month $\mathrm{SOS_2}$, a new growing cycle is initiated immediately after the last date of $\mathrm{SOS_2}$.
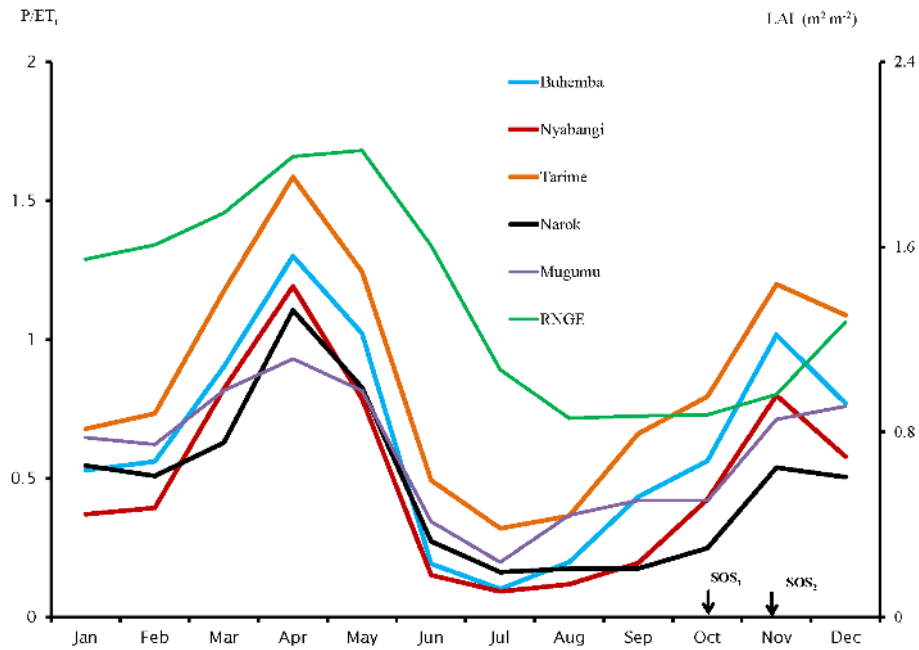
Figure 2. The moisture index (SMI) derived from historical precipitation observations (P) across the Mara Basin and the global reference evapotranspiration data of Trabucco and Zomer (2009) (ET_r). The dotted line represents the leaf area index (LAI) for the savanna ecosystem. SOS_1 and SOS_2 represent the start of the wet season (SOS) transition months to trigger growth.

Table 1. Summary of the inputs of the SWAT model and the evaluation datasets.

	Spatial/temporal resolution	Source	Description
Rainfall	5 km/1-day	Roy et al. (2017)	Bias-corrected satellite rainfall for Mara Basin
Climate	25 km/3 h	Rodell et al. (2004)	Max. and min. temperature, relative humidity, wind, solar radiation
Land cover classes	30 m	FAO (2002)	Land cover classes for east Africa
DEM	30 m	NASA (2014)	Digital elevation model
Soil classes	1 km	FAO (2009)	Global soil classes
Discharge	Daily (2002–2008)	WRMA (Kenya)	River discharge at Bomet
ET	1 km/8-day	Alemayehu et al. (2017)	ET maps for Mara Basin
MOD15A2	1 km/8-day	LPDAAC (2014)	Global leaf area index

It is worth noting that the SMI threshold can be set depending on the climatic condition of the basin.

The SWAT-T executable and the associated changes can be found in the Supplement.

2.7 The data used for the evaluations

2.7.1 The leaf area index

The remote sensing LAI data used in this study are based on the MODIS TERRA sensor (Table 1). The LAI product retrieval algorithm is based on the physics of the radiative transfer in vegetation canopies (Myneni et al., 2002) and involves several constants (leaf angle distribution, optical properties of soils and wood, and canopy heterogeneity) (Bobée

et al., 2012). The theoretical basis of the MODIS LAI algorithm and the validation results are detailed in Myneni et al. (2002). Kraus (2008) validated the MOD15A2 LAI data at the Budongo Forest (Uganda) and Kakamega Forest (Kenya) sites and reported an accuracy level comparable to the accuracy of field measurements, indicating the reliability of MOD15A2 LAI.

We selected relatively homogeneous representative sample sites (i.e. polygons) for evergreen forest ($174\,km^2$), tea ($123\,km^2$), savanna grassland ($136\,km^2$) and shrubland ($130\,km^2$) (see Fig. 1b) using the Africover classes and Google Earth images. This is useful to reduce the effect of mixed LAI values from different land cover classes while averaging the coarse-scale (i.e. 1 km) MODIS LAI. The MOD15A2 pixels with quality flag 0 (i.e. indicating good
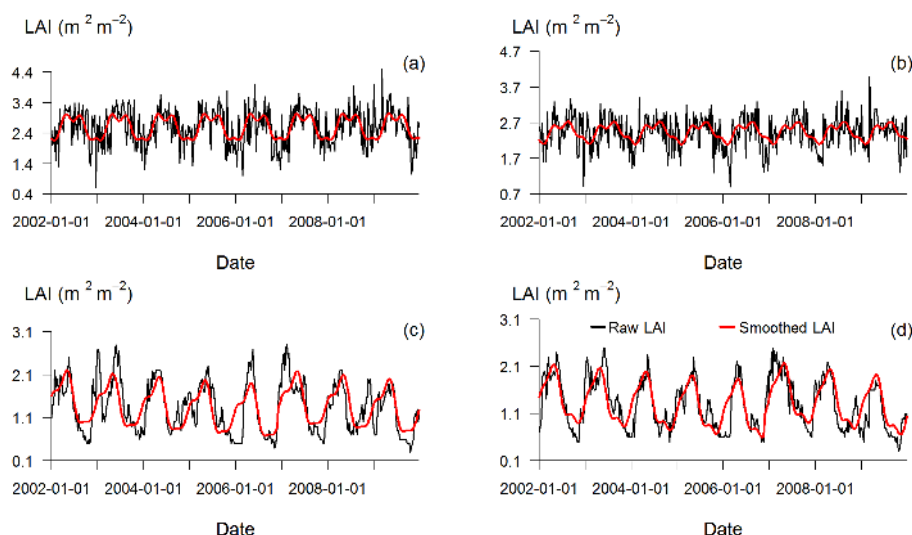
Figure 3. The 8-day raw-median LAI time series for evergreen forest **(a)**, tea **(b)**, grassland **(c)** and shrubland **(d)** sample sites. The raw-median LAI is smoothed using the Breaks For Additive Seasonal and Trend (BFAST) method (Verbesselt et al., 2010).

quality) were masked using the polygons of the sample covers. Also, pixels with LAI values less than 1.5 during the peak growing months (i.e. the period with LAI values mostly above 2.0) were removed. Finally, we extracted the 8-day median LAI time series for each land cover for 2002–2009 and few gaps in the LAI time series were filled using linear interpolation. Notwithstanding all the quality control efforts, we noted breaks and a high temporal variation in the LAI time series due the inevitable signal noise (Fig. 3). Verbesselt et al. (2010) developed the Breaks For Additive Seasonal and Trend (BFAST) method that decomposes the NDVI time series into trend, seasonal and remainder components. The trend and seasonal components comprise information that is pertinent to phenological developments as well as gradual and abrupt changes, whereas the remainder time series. This method has been applied to tropical ecosystems to identify phenological cycles as well as abrupt changes (DeVries et al., 2015; Verbesselt et al., 2010, 2012). In our study, we used the BFAST tool to extract the seasonal development pattern of LAI while excluding the noise and error information from the LAI time series. Figure 3 demonstrates the smoothed 8-day LAI time series using BFAST along with the raw-median LAI values. It is apparent from the smoothed LAI time series that the high LAI development occurs during the wet months from March to May, suggesting consistency in the smoothed LAI time series. Therefore, the smoothed LAI time series were used to calibrate and evaluate the SWAT-T model vegetation growth module for simulating LAI.

2.7.2 The evapotranspiration

ET is one of the major components of a basin water balance that is influenced by the seasonal vegetation growth cycle. Thus, remote-sensing-based ET estimates can be used

to evaluate (calibrate) the SWAT-T model. Alemayehu et al. (2017) estimated ET for the Mara River basin using several MODIS thermal imageries and the Global Land Data Assimilation System (GLDAS) (Rodell et al., 2004) weather dataset from 2002 to 2009 at an 8-day temporal resolution based on the operational simplified surface energy balance (SSEBop) algorithm (Senay et al., 2013). The latter mainly depends on the remotely sensed land surface temperature and the grass reference evapotranspiration (Senay et al., 2013). Alemayehu et al. (2017) demonstrated that the SSEBop ET for the study area explained about 52, 63 and 81 % of the observed variability in the MODIS NDVI at 16-day, monthly and annual temporal resolution. Also, they suggested that the estimated ET can be used for hydrological model parameterization. Therefore, we used this remote-sensing-based ET estimate (hereafter ET-RS) to evaluate the SWAT-T-simulated ET at a land cover level.

2.7.3 Streamflow

Due to the limited availability of observed streamflow, we used daily observed streamflow series (2002–2008) for the headwater region ($700 \, \text{km}^2$) at the Bomet gauging station. The streamflow dataset is relatively complete, with about 11 % missing data distributed throughout the time series.

2.8 Model set-up, calibration and evaluation

2.8.1 The model set-up and data used

The Mara River basin was delineated using a high-resolution (30 m) digital elevation model (DEM) (NASA, 2014) in ArcSWAT2012 (revision 627). The basin was subdivided into 89 sub-basins to spatially differentiate areas of the basin dom-

inated by different land use and/or soil type with dissimilar impact on hydrology. Each sub-basin was further discretized into several HRUs. The model was set up for land use conditions representing the period 2002–2009. The land cover classes for the basin were obtained from the FAO Africover project (FAO, 2002). As shown in Fig. 1b, the dominant portion of the basin is covered by natural vegetation including savanna grassland, shrubland and evergreen forest. These land cover classes were assigned the characteristics of RNGE, RNGB and FRSE, respectively, in the SWAT plant database (Neitsch et al., 2011). We extracted the soil classes for the basin from the Harmonized Global Soil Database (FAO, 2008). A soil properties database for the Mara River basin was established using the soil water characteristics tool (SPAW; http://hydrolab.arsusda.gov/soilwater).

The list of hydroclimatological and spatial data used to drive the SWAT model is presented in Table 1. In situ measurements of rainfall and other climate variables are sparse, and thus bias-corrected multi-satellite rainfall analysis data from Roy et al. (2017) were used. The bias correction involves using historical gauge measurements and a downscaling to a 5 km resolution. Detailed information on the bias-correction and downscaling procedures can be found in Roy et al. (2017). The ET_r was computed in SWAT using GLDAS weather data (Rodell et al., 2004) based on the Penman–Monteith (Monteith, 1965) approach. To remove the biases in SWAT-computed ET_r compared to the observation-based monthly average (1950–2000) ET_r data from Trabucco and Zomer (2009), the GLDAS solar radiation were adjusted relatively per month and per sub-basin.

2.8.2 Model calibration and evaluation approach

The main purpose of this study is to explore the potential of the SMI to trigger a new vegetation growth cycle for tropical ecosystems. To evaluate the effect of the modification on the SWAT vegetation growth module, we initially intercompared simulated LAI from the modified (i.e. SWAT-T) and the standard plant growth module with varying management settings. This analysis involved uncalibrated simulations with the default SWAT model parameters, whereby the models thus only differ regarding the way the vegetation growth is simulated, and in terms of the management settings. It is worth noting that the aim of these simulations is mainly to expose the inconsistencies in the vegetation growth module structure of the original SWAT model. Afterwards, we calibrated the parameters related to the simulation of the LAI, the ET and the streamflow by trial and error, and expert knowledge for the SWAT-T model. Firstly, the SWAT parameters that control the shape, the magnitude and the temporal dynamics of LAI were adjusted to reproduce the 8-day MODIS LAI for each land cover class. Then, we adjusted the parameters that mainly control the streamflow and ET simulation, simultaneously using the daily observed streamflow and the 8-day ET-RS. One may put forward that the manual adjustment

may not be as robust as an automatic calibration as the latter explores a larger parameter space. However, the manual calibration is believed to be apt to illustrate the impact of the modification of the vegetation growth cycle and its effect on the water balance components. The SWAT-T model calibration and validation were done for 2002–2005 and 2006–2009, respectively.

2.8.3 The model performance metrics

The Pearson correlation coefficient (r) and the percent of bias (PBIAS; %bias) were used to evaluate the agreement between the simulated and the remote-sensing-based estimates of LAI and ET for each land cover class and for the evaluation of the streamflow simulations. Additionally, the model performance was evaluated using the Kling–Gupta efficiency (KGE) (Gupta et al., 2009), which provides a compressive assessment by taking the variability, the bias and the correlation into account in a multi-objective sense.

3 Results and discussion

3.1 The consistency assessment of the vegetation growth module without calibration

3.1.1 The LAI simulations

To highlight the added value of the modified vegetation growth module in SWAT-T for simulating the seasonal growth pattern of trees and perennials, we compared the daily simulated LAI of the standard SWAT2012 (revision 627) model and SWAT-T model. At this stage, the models were uncalibrated (i.e. based on default SWAT parameters).

Figures 4 and 5 present the monthly rainfall along with SWAT-simulated daily LAI for FRSE and RNGE using the standard vegetation growth module under different management settings as well as the modified version (i.e. SWAT-T). In the standard plant growth module, whereby the heat unit management option is selected ("heat unit" in Figs. 4 and 5), the start and the end of the vegetation growth cycle occur at the default fr_{PHU} values of 0.15 and 1.2, respectively. With this management setting, the simulated LAI is zero at the beginning of each simulation year for both types of vegetation cover, which does not correspond to the reality for FRSE and RNGE in tropical regions. Strauch and Volk (2013), Kilonzo (2014) and Mwangi et al. (2016) reported similar observations. In this respect, it may be noted that Mwangi et al. (2016) improved the SWAT LAI simulation for FRSE by using a fr_{PHU} value of 0.001 to start the growing season, with a minimum LAI of 3.0. However, this change is region specific and cannot be transferred.

As shown in Figs. 4 and 5, the simulation with the standard SWAT module can be partly improved by using a date scheduling ("date") for the start and the end of the vegetation growth cycle (i.e. instead of heat unit). Alternatively,
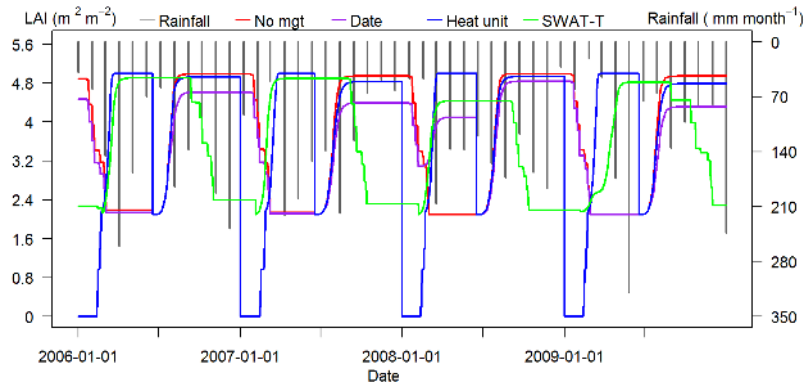
Figure 4. The daily LAI as simulated standard SWAT plant growth module with different management settings and by the modified plant growth module (SWAT-T) for evergreen forest (FRSE) using default SWAT parameters. The vertical lines (black) denote monthly rainfall (see management settings explanations in the text).
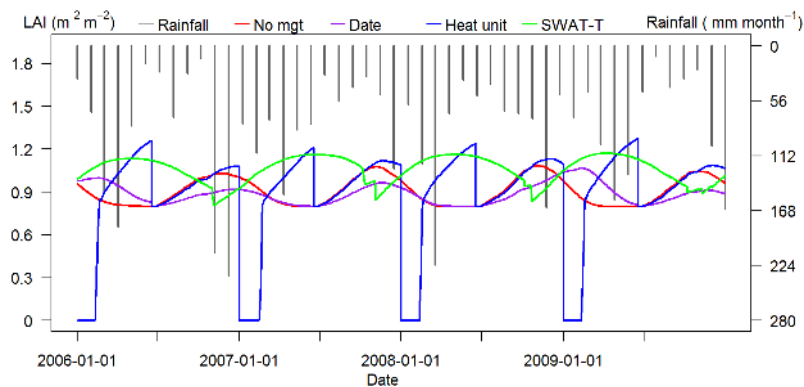

Figure 5. The daily LAI as simulated standard SWAT plant growth module with different management settings and by the modified plant growth module (SWAT-T) for grass (RNGE) using default SWAT parameters. The vertical lines (black) denote monthly rainfall (see management settings explanations in the text).

all the management settings can be removed ("no mgt") and vegetation can growing from the start of the simulation. It is worthwhile noting the low LAI values during and following the rainy months (i.e. March–May), suggesting unrealistic growth cycle simulation. Additionally, regardless of the management setting, the vegetation growth cycle resets annually on 28 June due to dormancy. In contrast, the simulated LAI with the modified vegetation growth module ("SWAT-T") corresponds with the monthly rainfall distribution, for FRSE and RNGE (see Figs. 4 and 5). We noted similar results for tea and RNGB.

3.1.2 The implication of inconsistent LAI simulation on the water balance components

In SWAT, the LAI is required to compute the potential transpiration, the potential soil evaporation and the plant biomass, among others. For instance, to compute the daily potential plant transpiration, the canopy resistance and the aerodynamic resistance are determined using the simulated LAI and the canopy height, respectively (Neitsch et al.,

2011). Therefore, the aforementioned limitations of the annual vegetation growth cycle in the standard SWAT model growth module also influence the simulation of the transpiration. Figure 6 shows a comparison of the daily potential transpiration for RNGE as simulated by the SWAT model with the standard and modified vegetation growth modules, based on the Penman–Monteith equation. We observe 12 % of the standard SWAT-simulated daily potential transpiration time series (2002–2009) for RNGE equal to zero, suggesting a considerable inconsistency. The inconsistency is considerably reduced when the modified vegetation growth module (SWAT-T) is used (i.e. less than 2 % zero values). Similar results are noted for FRSE and RNGB.

These findings should not come as a surprise as several studies have shown the effect of the selection of the ET_r method in SWAT on the simulated ET and other water balance components (Alemayehu et al., 2015; Maranda and Anctil, 2015; Wang et al., 2006). Alemayehu et al. (2015) reported substantial differences in both potential and actual transpiration with the choice of the ET_r method using a cali-
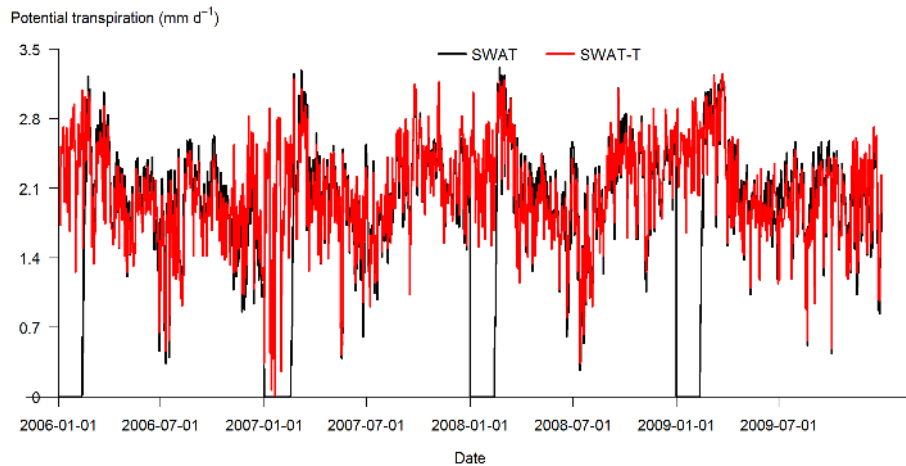
Figure 6. Comparison of Penman–Monteith-based daily potential transpiration simulated by the SWAT-T and the standard SWAT models for grassland. Note that the heat unit scheduling is used in the standard SWAT model.
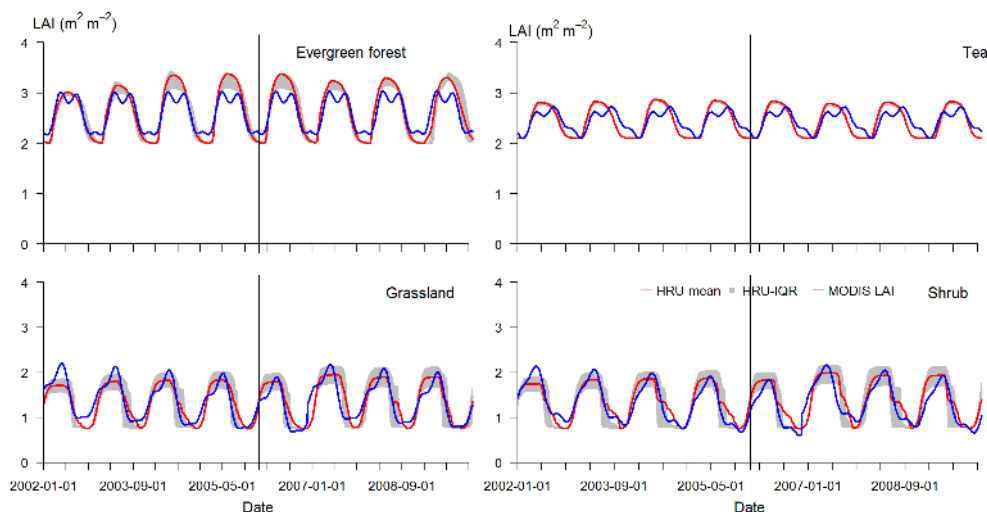

Figure 7. The MODIS LAI and the SWAT-T model-simulated, HRU-weighted, aggregated 8-day LAI time series (2002–2009). The grey shading indicate the boundaries of the 25th and 75th percentiles. The vertical line marks the end of the calibration period and the beginning of the validation period.

brated SWAT model, which was partly ascribed to the unrealistic LAI growth cycle.

We also notice the SWAT-T-simulated potential transpiration is consistent regardless of the ET_r method selection in SWAT (results not shown here), and therefore the improved vegetation growth module in the SWAT-T can reduce the uncertainty arising from the model structure and thus minimize the uncertainties in model simulation outputs.

3.2 The evaluation of the calibrated SWAT-T model

3.2.1 The performance of the LAI simulation

Table 2 presents the SWAT model parameters that are adjusted during the manual calibration process. Initially, the

minimum LAI (ALAI_MIN) for each land cover class was set based on the long-term MODIS LAI. Also, the PHU was computed using the long-term climatology, as suggested in Strauch and Volk (2013). The shape coefficients for the LAI curve (FRGW$_1$, FRGW$_2$, LAIMX$_1$, LAIMX$_2$ and DLAI) and the remaining parameters were adjusted during the calibration period by a trial-and-error process such that the SWAT-T-simulated 8-day LAI mimics the MODIS 8-day LAI.

Figure 7 presents the comparison of 8-day MODIS LAI with the calibrated SWAT-T-simulated LAI aggregated over several land cover classes for the calibration and validation periods. We evaluated the degree of agreement qualitatively (by visual comparison) and quantitatively (by statistical measures). From the visual inspection, it is apparent that the

Table 2. List of SWAT parameters used to calibrate LAI, ET and streamflow with their default and calibrated values.

Parameter	Parameter definition (unit)	Variable	Default (calibrated)		
			FRSE	RNGE	RNGB
BIO_E	Radiation-use efficiency ((kg/ha)/(MJ/m^2))	LAI	15 (17)	34 (10)	34 (10)
BLAI	Maximum potential leaf area index (m^2 m^{-2})	LAI	5 (4.0)	2.5 (3.5)	2 (3.5)
FRGW$_1$	Fraction of PHU corresponding to the first point on the optimal leaf area development curve	LAI	0.15 (0.06)	0.05 (0.2)	0.05 (0.2)
LAIMX$_1$	Fraction of BLAI corresponding to the first point on the optimal leaf area development curve	LAI	0.7 (0.15)	0.1 (0.1)	0.1 (0.1)
FRGW$_2$	Fraction of PHU corresponding to the second point on the optimal leaf area development curve	LAI	0.25 (0.15)	0.25 (0.5)	0.25 (0.5)
LAIMX$_2$	Fraction of BLAI corresponding to the second point on the optimal leaf area development curve	LAI	0.99 (0.30)	0.7 (0.99)	0.7 (0.99)
DLAI	Fraction of total PHU when leaf area begins to decline	LAI	0.99 (0.30)	0.35 (0.99)	0.35 (0.99)
T_OPT	Optimal temperature for plant growth (°C)	LAI	30 (25)	25 (30)	25 (30)
T_BASE	Minimum temperature for plant growth (°C)	LAI	0 (5)	12 (5)	12 (5)
ALAI_MIN	Minimum leaf area index for plant during dormant period (m^2 m^2)	LAI	0.75 (2.0)	0 (0.75)	0 (0.75)
PHU	Total number of heat units needed to bring plant to maturity	LAI	1800 (3570)	1800 (4100)	1800 (4100)
SOL_Z[a]	Soil layer depths (mm)	ET	300 [1000] (480 [1600])	300 [1000] (480 [1600])	300 [1000] (480 [1600])
SOL_AWC[b]	Soil available water (mm)	ET/flow	0.26–0.31 [0.27–0.29] (0.18–0.21 [0.18–0.20])	0.26–0.31 [0.27–0.29] (0.18–0.21 [0.18–0.20])	0.26–0.31 [0.27–0.29] (0.18–0.21 [0.18–0.20])
ESCO	Soil evaporation compensation factor (–)	ET	0.95 (0.88)	0.95 (1)	0.95 (1)
EPCO	Plant uptake compensation factor (–)	ET	1 (1)	1 (1)	1 (1)
GSI	Maximum stomatal conductance at high solar radiation and low vapour pressure deficit (m s^{-1})	ET	0.002 (0.006)	0.005 (0.0035)	0.005 (0.004)
REVAPMN	Depth of water in the aquifer for revap (mm)	ET	750 (100)	750 (100)	750 (100)
CN2[c]	Initial SCS curve number II value (–)	flow	55 [70] (38 [48])	69 [79] (81 [92])	61 [74] (71 [87])
SURLAG	Surface runoff lag time (day)	flow	4(0.01)	4(0.01)	4(0.01)
ALPHA_BF	Baseflow recession constant (day)	flow	0.048 (0.2)	0.048 (0.2)	0.048 (0.2)
GWQMN	Shallow aquifer minimum level for base flow	flow	1000 (50)	1000 (50)	1000 (50)
GW_REVAP	Groundwater "revap" coefficient (–)	ET	0.02 (0.1)	0.02 (0.02)	0.02 (0.02)
RCHRG_DP	Deep aquifer percolation fraction (–)	flow	0.05 (0.3)	0.05 (0.1)	0.05 (0.1)

[a] SOL_Z values for the top (and lower) soil layers depth. [b] SOL_AWC values range for the top (and lower) soil layers depending on soil texture and bulk density. [c] CN2 values for soil hydrologic group B(C).

intra-annual LAI dynamics (and hence the annual growth cycle of each land cover class) from the SWAT-T model corresponds well with the MODIS LAI data. This observation is supported by correlations as high as 0.94 (FRSE) and 0.92 (RNGB) during the calibration period (Table 3). As shown in Table 3, the model also shows a similar performance during the validation period, with low average bias and correlation

as high as 0.93 (FRSE). Overall, the results indicate that the SMI can indeed be used to dynamically trigger a new growing season within a predefined period.

Despite the overall good performance of SWAT-T in simulating the LAI, we observed biases for FRSE and tea, mainly during the rainy season (see top row of Fig. 7). This is partly attributed to the cloud contamination of the MODIS LAI in

Table 3. Summary of the performance metrics for the SWAT-T for simulating LAI, ET and streamflow. Note that the performance for LAI and ET refers to 8-day aggregated data, whereas daily streamflow data are considered.

	LAI calibration (validation)				ET calibration (validation)				Streamflow calibration (validation)
	FRSE	Tea	RNGE	RNGB	FRSE	Tea	RNGE	RNGB	Flow
r	0.94 (0.93)	0.83 (0.83)	0.89 (0.86)	0.92 (0.88)	0.71 (0.68)	0.67 (0.64)	0.72 (0.77)	0.66 (0.72)	0.72 (0.76)
%bias	1.5 (0)	0.1 (0.2)	−3.7 (−0.4)	−1.3 (4.6)	3.7 (6.6)	−1.7 (0.5)	7.8 (11)	1.2 (2.9)	3.5 (15.5)
KGE	0.50 (0.62)	0.42 (0.44)	0.86 (0.85)	0.88 (0.86)	0.71 (0.67)	0.62 (0.62)	0.69 (0.74)	0.66 (0.72)	0.71 (0.71)
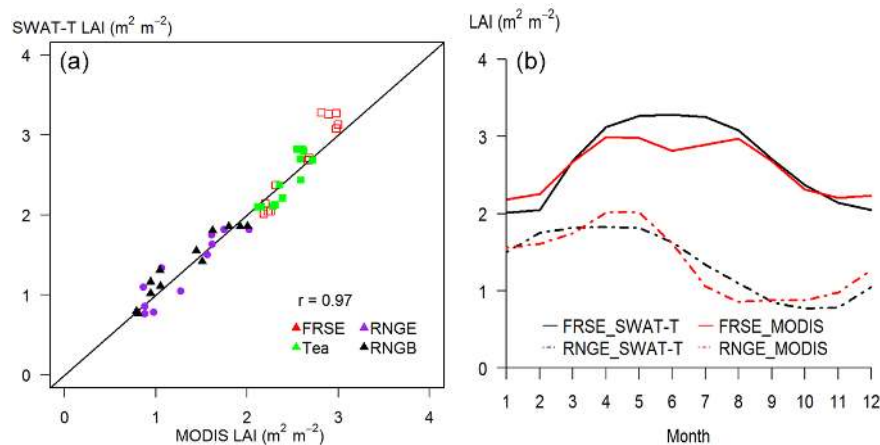
Figure 8. The long-term (2002–2009) average monthly LAI pooled scatter plot **(a)** and temporal dynamics **(b)**. FRSE: evergreen forest; RNGE: grassland; RNGB: shrubland.

the mountainous humid part of the basin, as shown in Fig. 3a and b. Similar observations were also made by Kraus (2008). Also, the senescence seems to occur slightly early for tea (see Fig. 3b), whereby we note a mismatch between the SWAT-simulated LAI and the MODIS LAI. This suggests the need to further adjust the fraction of total PHU when the leaf area begins to decline (DLAI).

3.2.2 The seasonal vegetation growth pattern

The seasonal patterns of the LAI for FRSE, tea, RNGE and RNGB are analysed using 8-day aggregated LAI data time series (2002–2009) from the calibrated SWAT-T model and MODIS LAI. Generally, and not surprisingly, the seasonal dynamics of the SWAT-T-simulated LAI and the MODIS LAI agree well (Fig. 8a) with a pooled correlation of 0.97.

As shown in Fig. 8b, the SWAT-T-simulated monthly average LAI shows a higher seasonal variation as compared to the variation observed from MODIS LAI for FRSE; the peak-to-trough difference of the SWAT-T data is about 48 % of the average annual MODIS LAI, while the amplitude is 31 % for the MODIS data. The seasonal variation from MODIS LAI is comparable to the results of Myneni et al. (2007), who noted 25 % seasonal variation in the Amazon forest. We also notice a correlation of 0.66 between the seasonal LAI and the rainfall in the humid part of the basin. Our observations are in

agreement with Kraus (2008), who reported an association of the LAI dynamics for forest sites located in Kenya and Uganda with interannual climate variability.

In the part of the basin where there is a marked dry season, the LAI exhibits a notable seasonal variation, with an amplitude that is up to 79 % of the mean annual LAI ($1.4\,\mathrm{m^2\,m^{-2}}$) for RNGE. Unlike the LAI of FRSE and tea in the humid part, the seasonal rainfall pattern is strongly correlated ($r = 0.81$) with lagged LAI for RNGE and RNGB. This result is in agreement with several studies that noted that the LAI dynamics for natural ecosystems in Sub-Saharan Africa are associated with the rainfall distribution pattern (Bobée et al., 2012; Kraus et al., 2009; Pfeifer et al., 2014).

In addition to improving the seasonal dynamics of LAI in SWAT without the need for management settings, the SMI accounts for the year-to-year shifts in the SOS due to climatic variations. This is particularly important for long-term land use change and climate change impact studies. Figure 9 demonstrates the year-to-year shifts as well as the spatial variation of the SOS dates for part of the Mara River basin dominated by savanna grassland. Generally, the season change tends to occur in the month of October (i.e. Julian date 278–304). Yet, we acknowledge the need of further verification studies in basins with sufficient forcing data and field measurements.
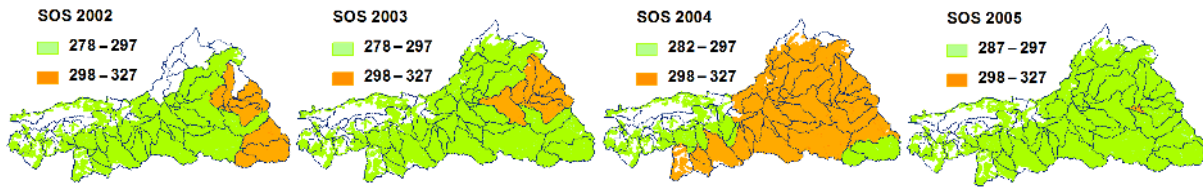
Figure 9. The interannual and spatial variation of the start of the rainy season for the savanna vegetation in the Mara River basin for 2002–2005. Note that HRU level Julian dates are used and the sub-basins are overlaid.
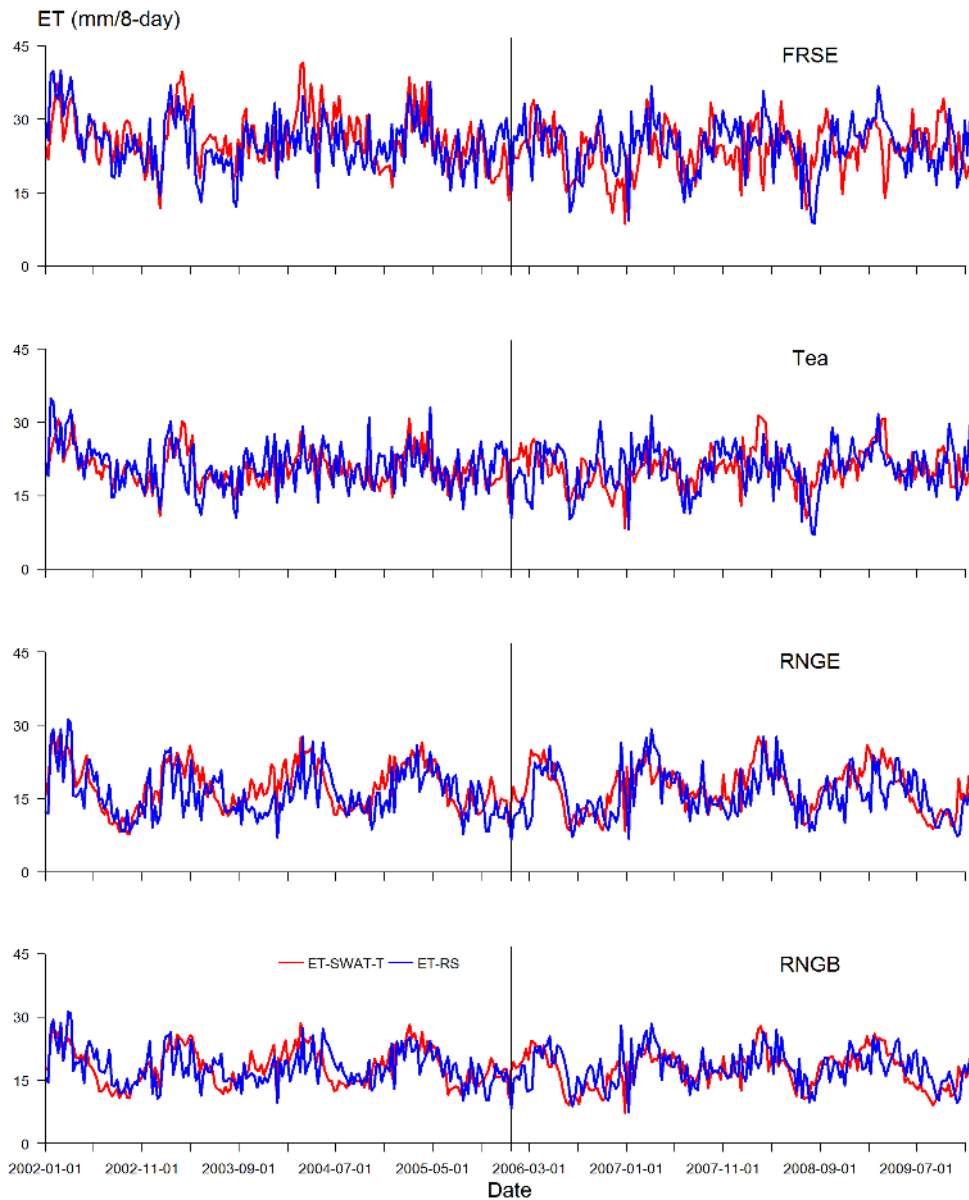

Figure 10. The comparison of remote-sensing-based evapotranspiration (ET-RS) and SWAT-T-simulated ET (ET-SWAT-T) aggregated per land cover class. Note that for SWAT-T HRU level ET is aggregated per land cover. The vertical black lines mark the end of the calibration period and the beginning of the validation period.
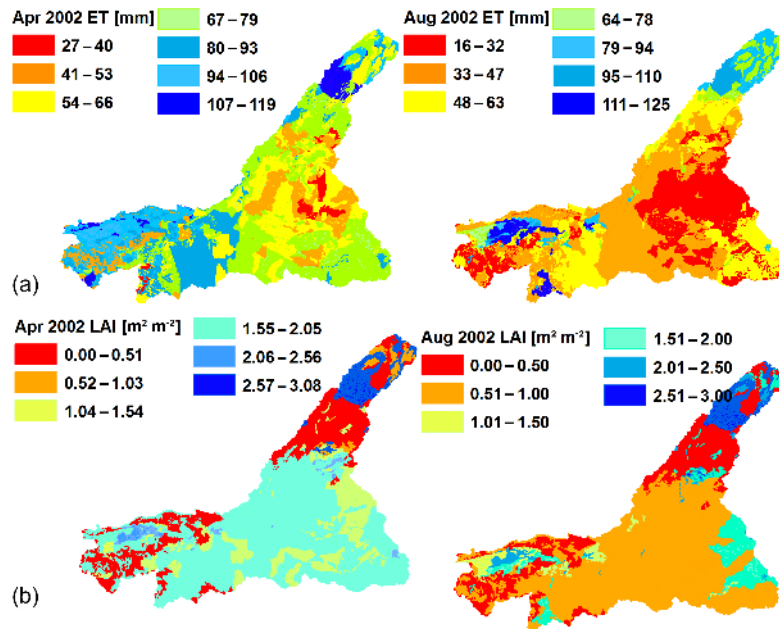
Figure 11. SWAT-T-simulated monthly ET **(a)** and LAI **(b)** for April (wet) and August (dry) 2002 at HRU level.

3.2.3 The spatial simulation of the evapotranspiration

As presented in Table 2, several SWAT parameters were calibrated by comparing SWAT-T model simulated ET with ET-RS. The higher water use by FRSE as compared to other land cover classes is reflected by a lower ESCO and a higher GW_REVAP and GSI (Table 2). The lower ESCO indicates an increased possibility of extracting soil water to satisfy the atmospheric demand at a relatively lower soil depth. Also, the higher GW_REVAP points to an increased extraction of water by deep-rooted plants from the shallow aquifer or pumping. Similar findings were reported by Strauch and Volk (2013).

Figure 10 presents the comparison of 8-day ET-RS and SWAT-T-simulated ET for the calibration (2002–2005) and validation (2006–2009) periods for FRSE, tea, RNGE and RNGB. Visually, the ET simulated by the SWAT-T fairly agrees with the ET-RS for all the covers. As shown in Table 3, the statistical performance indices show a modest performance in simulating ET for the dominant cover types in the basin. The average model biases for the simulated ET range from 7.8 % (RNGE) to 1.2 % (RNGB) during the calibration period. Additionally, the correlation between 8-day ET from the SWAT-T and the ET-RS varies from 0.67 (tea) to 0.72 (grassland). Overall, we notice similar performance measures during the calibration and validation periods, suggesting a fair representation of the processes pertinent to ET.

The variability of the ET is controlled by several biotic and abiotic factors. The 8-day ET time series as simulated by the SWAT-T model illustrates the variation of the temporal dynamics of ET in the study area. For land cover types

located in the humid part of the basin (FRSE and tea), there is no clear temporal pattern (Fig. 10). In contrast, the areas covered by RNGE and RNGB show a clear seasonality of the simulated ET. These observations are consistent with the seasonality of the simulated LAI, as discussed in Sect. 3.2.2.

To shed light on the consistency of SWAT-T-simulated LAI and ET, we selected simulation outputs at HRU level for April and August (Figs. 11 and 12). Figure 11a exhibits the monthly ET at HRU level for the wet month (April) and the dry month (August) in 2002. The lower portion of the basin, with dominant savanna cover, experiences a monthly ET between 16 and 63 mm month^{-1} in August and between 41 and 93 mm month^{-1} in April. These estimates are also well reflected in the spatial distribution of the average monthly simulated LAI (Fig. 11b). We notice that the linear relationship between ET and LAI is stronger, in general, for grassland and shrubs than for evergreen forest and tea. The lower correlation for tea and evergreen forest could be partly attributed to the high evaporation contribution of the wet soil, as the upper portion of the basin receives ample rainfall all year round. Also, the tea harvesting activities in the upper part of the basin are not taken into account in the model. Finally, we observe that during the wet month the spatial variability of ET is higher than that of the LAI (Fig. 11). Further comparison research is needed to evaluate the added value of the improved vegetation growth module on spatial ET simulations compared to remote-sensing-based ET. This will be addressed in our ongoing research on ET evaluation.
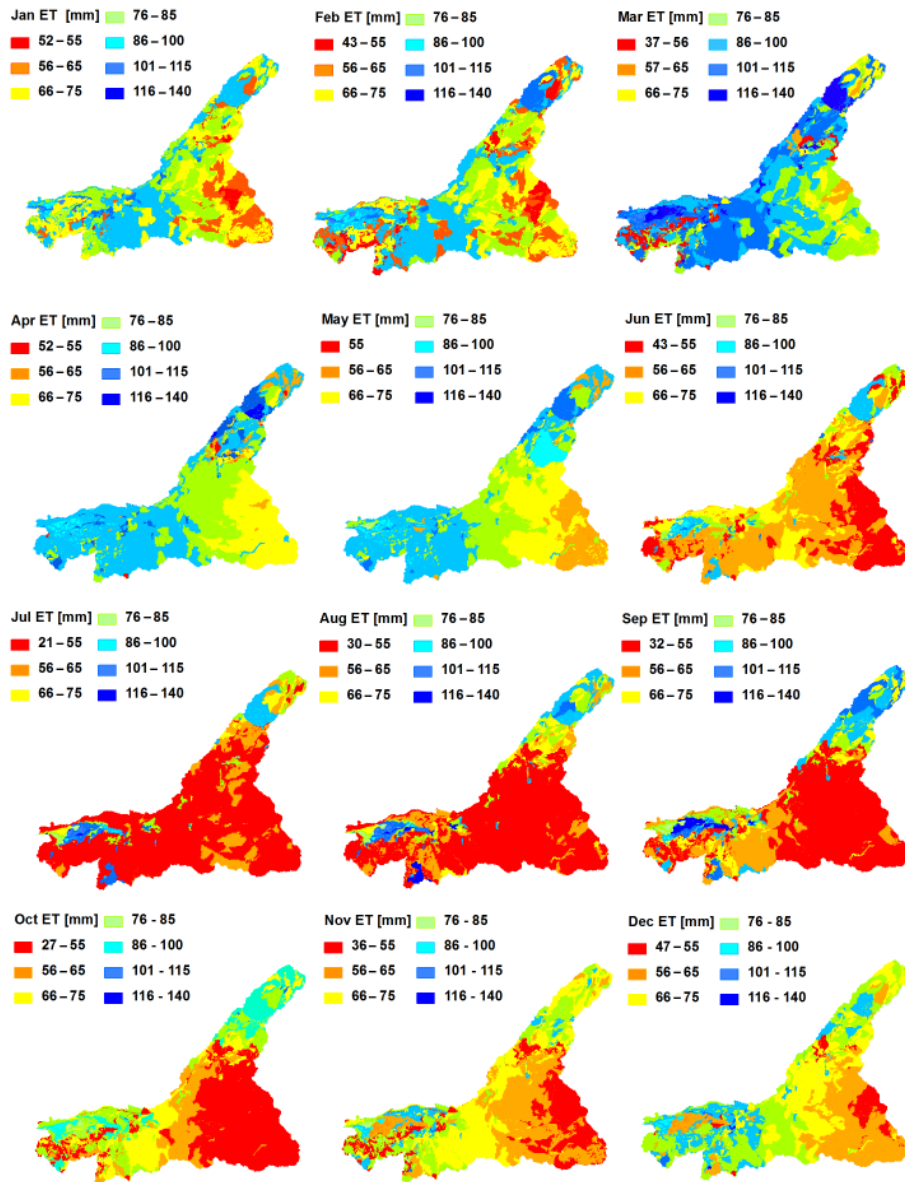
Figure 12. The average seasonal and spatial distribution of ET (2002–2009) in the Mara Basin, as simulated by the SWAT-T model at HRU level.

3.2.4 The performance of the streamflow simulations

Figure 13 presents the comparison of daily SWAT-T-simulated streamflow with observed streamflow, for the calibration and validation periods. Visually, the simulated hydrograph fairly reproduced the observations. The average biases of the SWAT-T-simulated streamflow as compared to observations amount to 3.5 and 15.5 % during the calibration and validation periods, respectively (Table 3). The correlation is about 0.72 (0.76) during calibration (validation) period. A KGE of 0.71 points to the overall ability of the calibrated SWAT-T model to reproduce the observed streamflow. However, the model tends to underestimate the baseflow and

this is more pronounced during the validation period. This is partly associated with the overestimation of the ET for evergreen forest (6.6 %) during the validation, since ET has a known effect on the groundwater flow.

4 Summary and conclusions

We presented an innovative approach to improve the simulation of the annual growth cycle for trees and perennials – and hence improve the simulation of the evapotranspiration and the streamflow – for tropical conditions in SWAT. The robustness of the changes made to the standard SWAT2012
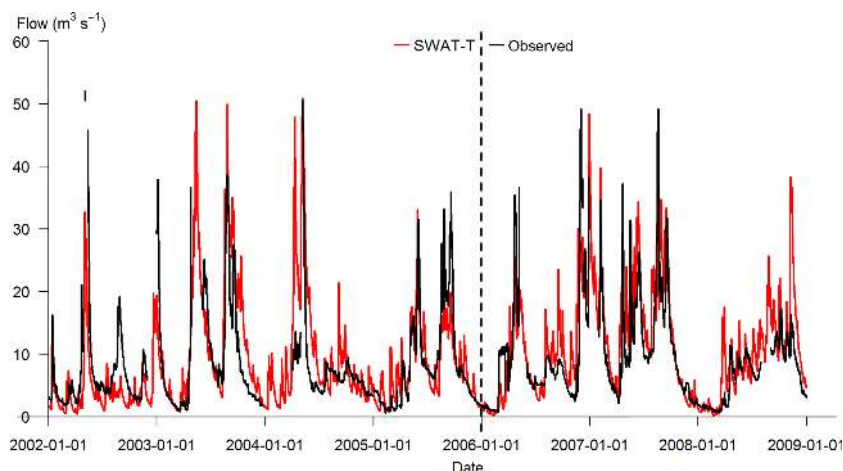
Figure 13. Observed and simulated flows for the Nyangores River at Bomet.

revision 627 have been assessed by comparing the model outputs with remotely sensed 8-day composite MODIS LAI data, as well as with remote-sensing-based evapotranspiration (ET-RS) and observed streamflow data. Towards this, we presented a straightforward but robust SMI, a quotient of rainfall (P) and reference evapotranspiration (ET_r), to trigger a new growing season within a predefined period. The new growing season starts when the SMI exceeds or equals a certain user-defined threshold.

The structural improvements of the LAI simulation have been demonstrated by comparing uncalibrated SWAT model simulations of the LAI using the modified (i.e. SWAT-T) and the standard SWAT vegetation growth module. The results indicate that the modified module structure for the vegetation growth exhibits temporal progression patterns that are consistent with the seasonal rainfall pattern in the Mara Basin. Further, we note a better consistency of the SWAT-T-simulated potential transpiration for perennials and trees, suggesting the usefulness of the vegetation growth module modification in reducing the model structural uncertainty. Our calibrated SWAT-T model results also show that the calibrated SWAT-T-simulated LAI corresponds well with the MODIS LAI for various land cover classes with correlations of up to 0.94, indicating the realistic representation of the start of the new growing season using the SMI within a predefined period. The improvement of the vegetation growth cycle in SWAT is also supported by a good agreement of the simulated ET with ET-RS, particularly for the grassland. Additionally, the daily streamflow simulated with the SWAT-T mimic well the observed streamflow for the Nyangores River. Therefore, the SWAT-T developed in this study can be a robust tool for simulating the vegetation growth dynamics in a consistent way in hydrologic model applications.

The Supplement related to this article is available online at https://doi.org/10.5194/hess-21-4449-2017-supplement.

References

Alemayehu, T., van Griensven, A., and Bauwens, W.: Evaluating CFSR and WATCH Data as Input to SWAT for the Estimation of the Potential Evapotranspiration in a Data-Scarce Eastern-African Catchment, J. Hydrol. Eng., 21, 5015028, https://doi.org/10.1061/(ASCE)HE.1943-5584.0001305, 2015.

Alemayehu, T., van Griensven, A., Senay, G. B., and Bauwens, W.: Evapotranspiration Mapping in a Heterogeneous Landscape Using Remote Sensing and Global Weather Datasets: Application to the Mara Basin, East Africa, Remote Sens., 9, 390, https://doi.org/10.3390/rs9040390, 2017.

Andersen, J., Dybkjaer, G., Jensen, K. H., Refsgaard, J. C., and Rasmussen, K.: Use of remotely sensed precipitation and leaf area

index in a distributed hydrological model, J. Hydrol., 264, 34–50, https://doi.org/10.1016/S0022-1694(02)00046-X, 2002.

Arnold, J. G., Srinivasan, R., Muttiah, R. S., and Williams, J. R.: Large area hydrologic modeling and assessment part I: model development, J. Am. Water Resour. As., 34, 73–89, https://doi.org/10.1111/j.1752-1688.1998.tb05961.x, 1998.

Arnold, J. G., Moriasi, D. N., Gassman, P. W., Abbaspour, K. C., White, M. J., Srinivasan, R., Santhi, C., Harmel, R. D., van Griensven, A., Van Liew, M. W., Kannan, N., and Jha, M. K.: SWAT: Model Use, Calibration, and Validation, T. ASABE, 55, 1491–1508, https://doi.org/10.13031/2013.42256, 2012.

Bobée, C., Ottlé, C., Maignan, F., De Noblet-Ducoudré, N., Maugis, P., Lézine, A. M., and Ndiaye, M.: Analysis of vegetation seasonality in Sahelian environments using MODIS LAI, in association with land cover and rainfall, J. Arid. Environ., 84, 38–50, https://doi.org/10.1016/j.jaridenv.2012.03.005, 2012.

Bressiani, D. de A., Gassman, P. W., Fernandes, J. G., Garbossa, L. H. P., Srinivasan, R., Bonumá, N. B., and Mendiondo, E. M.: A review of soil and water assessment tool (SWAT) applications in Brazil: Challenges and prospects, Int. J. Agric. Biol. Eng., 8, 1–27, https://doi.org/10.3965/j.ijabe.20150803.1765, 2015.

Dessu, S. B. and Melesse, A. M.: Modelling the rainfall-runoff process of the Mara River basin using the Soil and Water Assessment Tool, Hydrol. Process., 26, 4038–4049, https://doi.org/10.1002/hyp.9205, 2012.

DeVries, B., Verbesselt, J., Kooistra, L., and Herold, M.: Robust monitoring of small-scale forest disturbances in a tropical montane forest using Landsat time series, Remote Sens. Environ., 161, 107–121, https://doi.org/10.1016/j.rse.2015.02.012, 2015.

Easton, Z. M., Fuka, D. R., White, E. D., Collick, A. S., Biruk Ashagre, B., McCartney, M., Awulachew, S. B., Ahmed, A. A., and Steenhuis, T. S.: A multi basin SWAT model analysis of runoff and sedimentation in the Blue Nile, Ethiopia, Hydrol. Earth Syst. Sci., 14, 1827–1841, https://doi.org/10.5194/hess-14-1827-2010, 2010.

FAO: Africover Regional Land Cover Database, available at: http://www.africover.org (last access: 12 June 2015), 2002.

FAO: Harmonized World Soil Database (version 1.0), FAO, Rome, Italy a nd IIASA, Laxenburg, Austria, 2008.

FAO/IIASA/ISRIC/ISSCAS/JRC: Harmonized World Soil Database (version 1.1). FAO, Rome, Italy and IIASA, Laxenburg, Austria, 2009.

Gassman, P. W., Sadeghi, A. M., and Srinivasan, R.: Applications of the SWAT Model Special Section: Overview and Insights, J. Environ. Qual., 43, 1–8, https://doi.org/10.2134/jeq2013.11.0466, 2014.

Gebremicael, T. G., Mohamed, Y. A., Betrie, G. D., van der Zaag, P., and Teferi, E.: Trend analysis of runoff and sediment fluxes in the Upper Blue Nile basin: A combined analysis of statistical tests, physically-based models and landuse maps, J. Hydrol., 482, 57–68, https://doi.org/10.1016/j.jhydrol.2012.12.023, 2013.

Githui, F., Mutua, F., and Bauwens, W.: Estimating the impacts of land-cover change on runoff using the soil and water assessment tool (SWAT): case study of Nzoia catchment, Kenya/Estimation des impacts du changement d'occupation du sol sur l'écoulement à l'aide de SWAT: étude du cas du bassi, Hydrolog. Sci. J., 54, 899–908, https://doi.org/10.1623/hysj.54.5.899, 2009.

Gupta, H. V, Kling, H., Yilmaz, K. K., and Martinez, G. F.: Decomposition of the mean squared error and NSE performance criteria: Implications for improving hydrological modelling, J. Hydrol., 377, 80–91, https://doi.org/10.1016/j.jhydrol.2009.08.003, 2009.

Hargreaves, G. H. and Samani, Z. A.: Reference Crop Evapotranspiration from Temperature, Appl. Eng. Agric., 1, 96–99, https://doi.org/10.13031/2013.26773, 1985.

Jolly, W. M. and Running, S. W.: Effects of precipitation and soil water potential on drought deciduous phenology in the Kalahari, Glob. Change Biol., 10, 303–308, https://doi.org/10.1046/j.1365-2486.2003.00701.x, 2004.

Kilonzo, F.: Assessing the Impacts of Environmental Changes on the Water Resources of the Upper Mara, Lake Victoria Basin, PhD Thesis, Vrije Universiteit Brussel (VUB), 2014.

Kiniry, J. and MacDonald, J.: Plant growth simulation for landscape-scale hydrological modelling, Hydrolog. Sci. J., 53, 1030–1042, https://doi.org/10.1623/hysj.53.5.1030, 2008.

Kraus, T.: Ground-based Validation of the MODIS Leaf Area Index Product for East African Rain Forest Ecosystems, PhD thesis, Friedrich-Alexander University Erlangen-Nürnberg, Nürnberg, Germany, 2008.

Kraus, T., Schmidt, M., Dech, S. W., and Samimi, C.: The potential of optical high resolution data for the assessment of leaf area index in East African rainforest ecosystems, Int. J. Remote Sens., 30, 5039–5059, https://doi.org/10.1080/01431160903022878, 2009.

Krysanova, V. and White, M.: Advances in water resources assessment with SWAT – an overview, Hydrolog. Sci. J., 60, 1–13, https://doi.org/10.1080/02626667.2015.1029482, 2015.

Lotsch, A.: Coupled vegetation-precipitation variability observed from satellite and climate records, Geophys. Res. Lett., 30, 1774, https://doi.org/10.1029/2003GL017506, 2003.

LPDAAC: Land Processes Distributed Active Archive Center (LPDAAC) of NASA, available at: https://lpdaac.usgs.gov/data_access/data_pool (last access: 5 December 2014), 2014.

Mango, L. M., Melesse, A. M., McClain, M. E., Gann, D., and Setegn, S. G.: Land use and climate change impacts on the hydrology of the upper Mara River Basin, Kenya: results of a modeling study to support better resource management, Hydrol. Earth Syst. Sci., 15, 2245–2258, https://doi.org/10.5194/hess-15-2245-2011, 2011.

Maranda, B. and Anctil, F.: SWAT Performance as Influenced by Potential Evapotranspiration Formulations in a Canadian Watershed, T. ASABE, 58, 1585–1600, https://doi.org/10.13031/trans.58.11290, 2015.

McNally, A., Husak, G. J., Brown, M., Carroll, M., Funk, C., Yatheendradas, S., Arsenault, K., Peters-Lidard, C., and Verdin, J. P.: Calculating Crop Water Requirement Satisfaction in the West Africa Sahel with Remotely Sensed Soil Moisture, J. Hydrometeorol., 16, 295–305, https://doi.org/10.1175/JHM-D-14-0049.1, 2015.

Mengistu, D. T. and Sorteberg, A.: Sensitivity of SWAT simulated streamflow to climatic changes within the Eastern Nile River basin, Hydrol. Earth Syst. Sci., 16, 391–407, https://doi.org/10.5194/hess-16-391-2012, 2012.

Monteith, J. L.: Evaporation and the environment, The state and movement of water in living organisms, in: XIXth symposium, Cambridge University Press, Swansea, 1965.

Mwangi, H. M., Julich, S., Patil, S. D., McDonald, M. A., and Feger, K.-H.: Modelling the impact of agroforestry on hydrol-

ogy of Mara River Basin in East Africa, Hydrol. Process., 30, 3139–3155, https://doi.org/10.1002/hyp.10852, 2016.

Myneni, R., Hoffman, S., Knyazikhin, Y., Privette, J., Glassy, J., Tian, Y., Wang, Y., Song, X., Zhang, Y., Smith, G., Lotsch, A., Friedl, M., Morisette, J., Votava, P., Nemani, R., and Running, S.: Global products of vegetation leaf area and fraction absorbed PAR from year one of MODIS data, Remote Sens. Environ., 83, 214–231, https://doi.org/10.1016/S0034-4257(02)00074-3, 2002.

Myneni, R. B., Yang, W., Nemani, R. R., Huete, A. R., Dickinson, R. E., Knyazikhin, Y., Didan, K., Fu, R., Negron Juarez, R. I., Saatchi, S. S., Hashimoto, H., Ichii, K., Shabanov, N. V., Tan, B., Ratana, P., Privette, J. L., Morisette, J. T., Vermote, E. F., Roy, D. P., Wolfe, R. E., Friedl, M. A., Running, S. W., Votava, P., El-Saleous, N., Devadiga, S., Su, Y., and Salomonson, V. V.: Large seasonal swings in leaf area of Amazon rainforests, P. Natl. Acad. Sci. USA, 104, 4820–4823, https://doi.org/10.1073/pnas.0611338104, 2007.

NASA: United States Geological Survey Earth Explorer, available at: http://earthexplorer.usgs.gov/ (last access: 9 September 2015), 2014.

Neitsch, S. L., Arnold, J. G., Kiniry, J. R., and Williams, J. R.: Soil & Water Assessment Tool Theoretical Documentation Version 2009, Texas Water Resources Institute Technical Report No. 406 Texas A&M University System College Station, TX, 647 pp., 2011.

Pfeifer, M., Gonsamo, A., Disney, M., Pellikka, P., and Marchant, R.: Leaf area index for biomes of the Eastern Arc Mountains: Landsat and SPOT observations along precipitation and altitude gradients, Remote Sens. Environ., 118, 103–115, https://doi.org/10.1016/j.rse.2011.11.009, 2012.

Pfeifer, M., Lefebvre, V., Gonsamo, A., Pellikka, P. K. E., Marchant, R., Denu, D., and Platts, P. J.: Validating and linking the GIMMS leaf area index (LAI3g) with environmental controls in tropical Africa, Remote Sens., 6, 1973–1990, https://doi.org/10.3390/rs6031973, 2014.

Priestley, C. H. B. and Taylor, R. J.: On the Assessment of Surface Heat Flux and Evaporation Using Large-Scale Parameters, Mon. Weather Rev., 100, 81–92, https://doi.org/10.1175/1520-0493(1972)100<0081:OTAOSH>2.3.CO;2, 1972.

Ritchie, J. T.: Model for predicting evaporation from a row crop with incomplete cover, Water Resour. Res., 8, 1204–1213, https://doi.org/10.1029/WR008i005p01204, 1972.

Rodell, M., Houser, P. R., Jambor, U., Gottschalck, J., Mitchell, K., Meng, C.-J., Arsenault, K., Cosgrove, B., Radakovich, J., Bosilovich, M., Entin, J. K., Walker, J. P., Lohmann, D., and Toll, D.: The Global Land Data Assimilation System, B. Am. Meteorol. Soc., 85, 381–394, https://doi.org/10.1175/BAMS-85-3-381, 2004.

Roy, T., Serrat-Capdevila, A., Gupta, H., and Valdes, J.: A platform for probabilistic Multimodel and Multiproduct Streamflow Forecasting, Water Resour. Res., 3, 1–24, https://doi.org/10.1002/2016WR019752, 2017.

Sacks, W. J., Deryng, D., Foley, J. A. and Ramankutty, N.: Crop planting dates: an analysis of global patterns, Global Ecol. Biogeogr., 19, 607–620, https://doi.org/10.1111/j.1466-8238.2010.00551.x, 2010.

Senay, G. B., Bohms, S., Singh, R. K., Gowda, P. H., Velpuri, N. M., Alemu, H., and Verdin, J. P.: Operational Evapotranspiration

Mapping Using Remote Sensing and Weather Datasets: A New Parameterization for the SSEB Approach, J. Am. Water Resour. As., 49, 577–591, https://doi.org/10.1111/jawr.12057, 2013.

Setegn, S. G., Srinivasan, R., Melesse, A. M., and Dargahi, B.: SWAT model application and prediction uncertainty analysis in the Lake Tana Basin, Ethiopia, Hydrol. Process., 24, 357–367, https://doi.org/10.1002/hyp.7457, 2009.

Setegn, S. G., Rayner, D., Melesse, A. M., Dargahi, B., and Srinivasan, R.: Impact of climate change on the hydroclimatology of Lake Tana Basin, Ethiopia, Water Resour. Res., 47, W04511, https://doi.org/10.1029/2010WR009248, 2011.

Shen, C., Niu, J., and Phanikumar, M. S.: Evaluating controls on coupled hydrologic and vegetation dynamics in a humid continental climate watershed using a subsurface-land surface processes model, Water Resour. Res., 49, 2552–2572, https://doi.org/10.1002/wrcr.20189, 2013.

Strauch, M. and Volk, M.: SWAT plant growth modification for improved modeling of perennial vegetation in the tropics, Ecol. Modell., 269, 98–112, https://doi.org/10.1016/j.ecolmodel.2013.08.013, 2013.

Teklesadik, A. D., Alemayehu, T., van Griensven, A., Kumar, R., Liersch, S., Eisner, S., Tecklenburg, J., Ewunte, S., and Wang, X.: Inter-model comparison of hydrological impacts of climate change on the Upper Blue Nile basin using ensemble of hydrological models and global climate models, Climatic Change, 141, 517–532, https://doi.org/10.1007/s10584-017-1913-4, 2017.

Trabucco, A. and Zomer, R. J.: Global Aridity Index (Global-Aridity) and Global Potential Evapo-Transpiration (Global-PET) Geospatial Database, CGIAR Consortium for Spatial Information, available from the CGIAR-CSI GeoPortal, available at: http://www.cgiar-csi.org/data/ (last access: 20 January 2015), 2009.

USDA SCS: Section 4 Hydrology, National Engineering Handbook, Washington, 1972.

van Griensven, A., Ndomba, P., Yalew, S., and Kilonzo, F.: Critical review of SWAT applications in the upper Nile basin countries, Hydrol. Earth Syst. Sci., 16, 3371–3381, https://doi.org/10.5194/hess-16-3371-2012, 2012.

Verbesselt, J., Hyndman, R., Newnham, G., and Culvenor, D.: Detecting trend and seasonal changes in satellite image time series, Remote Sens. Environ., 114, 106–115, https://doi.org/10.1016/j.rse.2009.08.014, 2010.

Verbesselt, J., Zeileis, A., and Herold, M.: Near real-time disturbance detection using satellite image time series, Remote Sens. Environ., 123, 98–108, https://doi.org/10.1016/j.rse.2012.02.022, 2012.

Verdin, J. and Klaver, R.: Grid-cell-based crop water accounting for the famine early warning system, Hydrol. Process., 16, 1617–1630, https://doi.org/10.1002/hyp.1025, 2002.

Wagner, P. D., Kumar, S., Fiener, P. and Schneider, K.: Hydrological Modeling with SWAT in a Monsoon-Driven environment: Experience from the Western Ghats, India, T. ASABE, 54, 1783–1790, 2011.

Wang, X., Melesse, A. M., and Yang, W.: Influences of Potential Evapotranspiration Estimation Methods on SWAT's Hydrologic Simulation in a Northwestern Minnesota Watershed, T. ASABE, 49, 1755–1771, https://doi.org/10.13031/2013.22297, 2006.

Yang, Q. and Zhang, X.: Improving SWAT for simulating water and carbon fluxes of forest ecosystems, Sci. Total Environ., 569–570,

1478–1488, https://doi.org/10.1016/j.scitotenv.2016.06.238, 2016.

Yu, X., Lamačová, A., Duffy, C., Krám, P., and Hruška, J.: Hydrological model uncertainty due to spatial evapotranspiration estimation methods, Comput. Geosci., 90, 90–101, https://doi.org/10.1016/j.cageo.2015.05.006, 2016.

Zhang, K., Kimball, J. S., Nemani, R. R., and Running, S. W.: A continuous satellite-derived global record of land surface evapotranspiration from 1983 to 2006, Water Resour. Res., 46, 1–21, https://doi.org/10.1029/2009WR008800, 2010.

Zhang, X.: Monitoring the response of vegetation phenology to precipitation in Africa by coupling MODIS and TRMM instruments, J. Geophys. Res., 110, D12103, https://doi.org/10.1029/2004JD005263, 2005.

Zhang, X., Friedl, M. A., and Schaaf, C. B.: Global vegetation phenology from Moderate Resolution Imaging Spectroradiometer (MODIS): Evaluation of global patterns and comparison with in situ measurements, J. Geophys. Res.-Biogeo., 111, 1–14, https://doi.org/10.1029/2006JG000217, 2006.

Zhang, Y., Chiew, F. H. S., Zhang, L., and Li, H.: Use of Remotely Sensed Actual Evapotranspiration to Improve Rainfall–Runoff Modeling in Southeast Australia, J. Hydrometeorol., 10, 969–980, https://doi.org/10.1175/2009JHM1061.1, 2009.